The Astrophysical Journal, 714:1624–1636, 2010 May 10 doi:10.1088/0004-637X/714/2/1624

AN INVESTIGATION INTO THE ORIGIN OF Fe-RICH PRESOLAR SILICATES IN ACFER 094

Maitrayee Bose, Christine Floss, and Frank J. Stadermann
Laboratory for Space Sciences and Physics Department, Washington University, St. Louis, MO 63130, USA; mbose@physics.wustl.edu
Received 2009 October 5; accepted 2010 March 24; published 2010 April 21

ABSTRACT

Presolar silicate and oxide grains from primitive meteorites are recognized as "stardust" on the basis of their extremely anomalous O isotopic compositions. We report data on 48 O-anomalous grains that were identified in grain size separates of the ungrouped carbonaceous chondrite Acfer 094. A majority of these grains exhibit high $^{17}O/^{16}O$ isotopic ratios along with solar to sub-solar $^{18}O/^{16}O$ ratios and may have originated in low-mass stars with close-to-solar metallicity. Four silicate grains that contain ^{18}O enrichments were also measured for their Si isotopes. A comparison of their O and Si isotopic compositions with model predictions indicates that these ^{18}O-rich grains may have formed in supernova ejecta. Four of the O-anomalous grains are oxides while the remaining 44 are silicates, based on elemental compositions determined by Auger spectroscopy. The presolar oxides include a TiO_2 grain and a grain with spinel stoichiometry. The silicate grains largely exhibit ferromagnesian compositions, although a few grains also contain small amounts of Ca and/or Al. Stoichiometric silicates were further classified as either olivine-like or pyroxene-like, and in this study pyroxene-like grains are more abundant than olivine-like ones. The majority of silicates contain more Fe than Mg, including a few grains with Fe-rich end-member compositions. Spectroscopic observations indicate the presence of Mg-rich silicates in the atmospheres of stars and the interstellar medium. Mg-rich minerals such as forsterite and enstatite form by equilibrium condensation in stellar environments. However, non-equilibrium condensation can result in higher Fe contents and the occurrence of such processes in the outflows of stars may account for the Fe-rich grains. Alternatively, secondary processes may play a role in producing the Fe enrichments observed in the presolar silicate grains identified in the matrix of Acfer 094.

Key words: astrochemistry – circumstellar matter – stars: AGB and post-AGB – supernovae: general

Online-only material: color figure

1. INTRODUCTION

Small dust grains condense in the expanding atmospheres of red giant (RG) and asymptotic giant branch (AGB) stars as well as in the ejecta of supernovae (SNe). Some of them survived travel in the interstellar medium (ISM) and were included in the molecular cloud from which our solar system formed. The refractory dust grains that escaped homogenization in the solar nebula can be extracted from extraterrestrial samples, such as meteorites, by acid dissolution. The enormous variations in isotopic ratios of these grains compared to solar system materials indicate their stellar origins. The first presolar grains that were discovered in the laboratory were carbonaceous phases, including SiC (Bernatowicz et al. 1987) and graphite (Amari et al. 1990). In addition to C-rich dust, oxides, such as corundum and spinel have been identified (Huss et al. 1994; Hutcheon et al. 1994; Nittler et al. 1994, 1997). Comparison of the isotopic data for presolar oxide grains from meteorites with stellar observations and models of dust producing stars indicates that most of these grains formed in low-mass RG or AGB stars, with a small fraction having formed in SN ejecta (Choi et al. 1998; Nittler et al. 1997, 1998).

Spectroscopic observations of envelopes surrounding evolved stars (Waters et al. 1996; Demyk et al. 2000) and circumstellar disks around young stellar objects (Waelkens et al. 1996) indicate the presence of silicate minerals. In particular, the 9.7 and 18 μm emission features observed in O-rich stars have been attributed to amorphous silicates (e.g., Waters et al. 1996). However, amorphous silicates cannot fully account for the infrared emission from these stars; an additional crystalline component is required (e.g., Waelkens et al. 1996). Circumstellar silicate grains were first discovered in interplanetary dust particles (Messenger et al. 2003), followed by their identification in the primitive meteorites Acfer 094 and NWA 530 (Nguyen & Zinner 2004; Nagashima et al. 2004). Acfer 094 is classified as an ungrouped carbonaceous chondrite (Newton et al. 1995). The matrix of this meteorite is composed of fine-grained olivines, pyroxenes, Fe–Ni sulfides, and amorphous material (Greshake 1997), as well as abundant presolar SiC and nanodiamonds (Newton et al. 1995; Gao et al. 1996). Numerous studies have been carried out to search for presolar silicates in Acfer 094 (Nguyen & Zinner 2004; Mostefaoui & Hoppe 2004; Nagashima et al. 2004; Nguyen et al. 2007; Vollmer et al. 2009b) and estimates of the matrix-normalized abundance of such grains range from about 90 to 160 ppm (Nguyen et al. 2007; Vollmer et al. 2009b).

Recent studies demonstrate that coordinated isotopic and elemental analyses of presolar silicates in the laboratory can provide valuable insight into their formation in stellar environments (Floss et al. 2008; Floss & Stadermann 2009; Vollmer et al. 2009b). Here, we report on the O isotopic and elemental compositions of presolar silicates and oxides identified from grain size separates of Acfer 094. Preliminary results were reported in Bose et al. (2007, 2008a, 2008b).

2. METHODS

2.1. Sample Preparation

Grain size separates (0.1–0.5 μm and 0.5–1.0 μm) originally prepared by A. N. Nguyen were used for the measurements in this study. The procedure is discussed in detail in Nguyen (2005) and is briefly outlined here. A small fragment of Acfer 094 was placed in distilled water and disaggregated by a rapid "freeze-thaw" process, followed by ultrasonification. The

sample was then repeatedly washed in distilled water and soluble organic compounds, such as toluene, to remove precipitates that might have formed during the disaggregation process and to achieve optimal dispersion of the grains. Size separates of the grains were produced by repeated centrifugation, and the grains were then dispensed onto gold foils pressed into stainless steel stubs. Areas on the gold foils that were densely covered with grains were chosen for measurements in the NanoSIMS.

2.2. NanoSIMS Measurements

Oxygen isotopic measurements were done with a Cs^+ primary beam of a few pA in the Washington University NanoSIMS 50. The beam was rastered over 10×10 μm^2 or, in some cases, 20×20 μm^2 areas in an imaging mode (256^2 or 512^2 pixels). Secondary ions of $^{12}C^-$, $^{13}C^-$, $^{16}O^-$, $^{17}O^-$, and $^{18}O^-$ or $^{16}O^-$, $^{17}O^-$, $^{18}O^-$, $^{28}Si^-$, and $^{24}Mg^{16}O^-$ were measured in the multi-collection mode together with secondary electrons (SEs). The analyses consisted of multiple (5–25) scans, with analysis times of up to 20 minutes for each scan. The individual layers were added together to make a single image for each analyzed species. Isotopic compositions of the presolar grains were determined following the data reduction procedures discussed in Stadermann et al. (2005), assuming normal (solar) compositions for the bulk of the matrix grains analyzed ($^{17}O/^{16}O = 3.8 \times 10^{-4}$ and $^{18}O/^{16}O = 2.0 \times 10^{-3}$). A grain was considered presolar if at least one of its O isotopic ratios differed by more than 5σ from those of the normal grains and the anomaly was present in at least three consecutive layers.

Following the O isotopic analyses, four ^{18}O-enriched presolar grains were also measured for Si isotopes. For these measurements the Cs^+ beam was rastered over a 3×3 μm^2 area (256^2 pixels) centered on the grain, while detecting $^{16}O^-$, $^{18}O^-$, $^{28}Si^-$, $^{29}Si^-$, and $^{30}Si^-$ secondary ions for ten imaging scans. The Si isotopic ratios of the presolar grains were normalized by assuming that the surrounding material has solar ratios of $^{29}Si/^{28}Si$ (5.08×10^{-2}) and $^{30}Si/^{28}Si$ (3.36×10^{-2}). The normalized Si isotopic ratios were then computed as delta values, indicating deviations from solar ratios in parts per thousand.

Iron isotopic measurements were performed for two relatively large ($\sim 300 \times 200$ nm^2) grains using an O^- primary ion beam and combined analysis mode, in which multi-collection is combined with magnetic peak jumping; the details of the measurement procedure are described by Floss et al. (2008). A correction was made for the contribution of $^{54}Cr^+$ on $^{54}Fe^+$ and the Fe isotopic ratios were normalized to the average $^{54}Fe/^{56}Fe$ and $^{57}Fe/^{56}Fe$ ratios of surrounding isotopically normal silicate grains present on the grain mounts.

2.3. Auger Nanoprobe Measurements

The PHI 700 Auger Nanoprobe, which was recently installed at Washington University, was used to obtain the elemental compositions of the O-anomalous grains. Prior to acquiring spectra or elemental maps, controlled sputter cleaning with a diffuse 2 keV, 1 μA Ar^+ ion beam was done in order to remove surface contaminants. Iterative Auger electron energy spectra of the presolar grains were obtained at a primary beam accelerating voltage of 10 keV and a current of 0.25 nA in the energy range 30–1730 eV. The low current used during the measurements, combined with rastering the electron beam over the area of the grain, reduces the potential for beam damage to the grains (Stadermann et al. 2009). Multiple iterations of the spectra of a given grain were added together to obtain a single spectrum. The average spectrum was differentiated, using a seven-point Savitsky–Golay smoothing and differentiation routine, followed by identification of the elements on the basis of their characteristic peaks (Childs et al. 1995). Compositions of the grains are calculated from peak-to-peak heights in the differentiated spectra and are then corrected for elemental sensitivities. The sensitivity factors computed from repeated Auger measurements on powdered olivine and pyroxene standards, under the same analytical conditions as used in this study, are as follows: Ca, 0.626; O, 0.194; Fe, 0.150; Mg, 0.234; Al, 0.160; and Si, 0.121 (Stadermann et al. 2009). The Auger peaks used for quantification are the same as those specified in Stadermann et al. (2009), e.g., KLL transition peak of O and LMM peak of Fe. The sensitivity factors have the following 1σ uncertainties: Ca, 10.8%; O, 3.6%; Fe, 11.2%; Mg, 9.4%; Al, 24.9%; Si, 11.0% (Stadermann et al. 2009). The high uncertainty for Al reflects the fact that the standards measured to date contain relatively low concentrations of this element. Oxide grain compositions may have greater uncertainties associated with them because the sensitivity factors listed above were computed from measuring silicate mineral standards. Additional errors, such as those associated with the presence of surface contaminants, sample charging, and background noise, are not included in the reported errors, which should therefore be considered lower limits.

Information from the spectra was supplemented with Auger elemental distribution maps of the presolar grains and surrounding areas. Maps were acquired by rastering the areas of interest (3×3 μm^2 or 5×5 μm^2) at 10 keV and 10 nA for 5–30 scans. The elemental maps provide detailed qualitative information about the elements present in the grains, their spatial distribution, and possible contributions to the Auger spectra from surrounding grains.

3. RESULTS

Forty-eight O-anomalous presolar grains were identified in a total analyzed area of 42,000 μm^2 on the grain mounts. Grains were located in two size separates of Acfer 094: grains in the size range 0.1–0.5 μm have names that start with "42" and those in the size range 0.5–1.0 μm have names that start with "34," followed by the specific area on the mount (e.g., "F") and finally by grain names (e.g., "s8," "7," "e8O17").

3.1. Isotopic Compositions

Forty O-anomalous grains (i.e., 83%) exhibit ^{17}O enrichments of up to $\sim$7 times solar, with sub-solar to solar $^{18}O/^{16}O$ ratios (Table 1). These ^{17}O-rich grains (Figure 1) are classified as group 1 grains (Nittler et al. 1997). While there are no group 2 grains in our presolar grain inventory, which would have greater ^{18}O depletions than group 1 grains, there is a possibility that a few grains currently identified as group 1 actually belong to the group 2 category (discussed later in Section 4.1). Grains with ^{16}O-rich compositions do not exist in our inventory.

Four grains with ^{18}O excesses, classified as group 4 (Figure 1), were identified. The Si isotopic ratios of these grains are plotted in Figure 2. The grains have normal Si isotopic compositions within 1σ errors, except for grain 34A-4, which has a slight enrichment (64‰ ± 26‰) in ^{30}Si (Table 1).

Two group 1 grains that were measured for Fe isotopes have normal $^{54}Fe/^{56}Fe$ and $^{57}Fe/^{56}Fe$ isotopic ratios. Grain 42Fe14 has $\delta^{54}Fe/^{56}Fe = -107‰ \pm 53‰$ and $\delta^{57}Fe/^{56}Fe = -192‰ \pm 87‰$, and grain 42Ff11 has $\delta^{54}Fe/^{56}Fe = -113‰ \pm 46‰$ and $\delta^{57}Fe/^{56}Fe = -75‰ \pm 87‰$. Nickel isotopic ratios could not be calculated because count rates were too low.

Table 1
Oxygen and Silicon Isotopic Ratios and Grain Sizes of Presolar Silicate and Oxide Grains

Grain	Size (nm^2)	$^{17}O/^{16}O$ ($\times 10^{-4}$)	$^{18}O/^{16}O$ ($\times 10^{-3}$)	$\delta^{29}Si$ (‰)	$\delta^{30}Si$ (‰)	Group[a]
			Pyroxene-like silicates			
42Ff11O18	340 × 240	3.76 ± 0.22	2.42 ± 0.05	−32 ± 45	−22 ± 55	4
42Ff25O	200 × 140	6.60 ± 0.34	1.40 ± 0.05	...	...	1
42Fs13	300 × 200	4.84 ± 0.23	1.21 ± 0.04	...	...	1
42Ft13	180 × 160	6.20 ± 0.24	1.59 ± 0.04	...	...	1
42Ft14_I	310 × 150	5.35 ± 0.24	1.98 ± 0.05	...	...	1
42Ft24	290 × 200	5.63 ± 0.40	2.01 ± 0.08	...	...	1
34C-7*	190 × 190	8.14 ± 0.53	1.23 ± 0.06	...	...	1
42C-7*	190 × 155	8.80 ± 0.46	1.76 ± 0.06	...	...	1
42Fe8O18*	220 × 160	5.68 ± 0.51	1.30 ± 0.07	...	...	1
42Ff2*	200 × 200	4.92 ± 0.37	2.00 ± 0.07	...	...	1
42Ff12*	330 × 200	8.51 ± 0.49	2.03 ± 0.07	...	...	1
42Fv114_I*	400 × 300	7.99 ± 0.16	1.22 ± 0.02	...	...	1
			Olivine-like silicates			
42Fc3	290 × 120	6.16 ± 0.51	1.99 ± 0.09	...	...	1
42Fs8	120 × 100	7.42 ± 0.05	1.98 ± 0.03	...	...	1
42Fw3	200 × 120	6.29 ± 0.25	1.85 ± 0.04	...	...	1
42B-11*	150 × 150	3.61 ± 0.48	2.77 ± 0.13	4 ± 32	28 ± 38	4
42Ft21*	140 × 100	5.84 ± 0.37	1.95 ± 0.07	...	...	1
42Fu5*	270 × 180	5.63 ± 0.36	1.60 ± 0.06	...	...	1
			Intermediate silicates			
34C-5	190 × 270	7.38 ± 0.45	1.68 ± 0.07	...	...	1
42B-1	150 × 190	8.94 ± 0.47	1.09 ± 0.05	...	...	1
42F-11	230 × 230	8.07 ± 1.21	2.39 ± 0.22	...	...	1
42Fb2	160 × 120	6.32 ± 0.36	2.06 ± 0.06	...	...	1
42Fd6	320 × 160	6.65 ± 0.79	1.84 ± 0.13	...	...	1
42Fe2	200 × 180	5.96 ± 0.38	2.12 ± 0.07	...	...	1
42Fe5O17	140 × 140	7.13 ± 0.47	2.01 ± 0.07	...	...	1
42Fe8O17	240 × 90	27.01 ± 0.95	2.38 ± 0.08	...	...	1
42Fe13	200 × 140	11.31 ± 0.46	1.96 ± 0.06	...	...	1
42Ff3	250 × 80	4.97 ± 0.51	1.16 ± 0.07	...	...	1
42Ff5	200 × 140	4.28 ± 0.27	2.44 ± 0.06	48 ± 46	−10 ± 53	4
42Ff10	200 × 200	9.39 ± 0.85	1.96 ± 0.12	...	...	1
42Fv115	210 × 170	4.86 ± 0.21	1.90 ± 0.04	...	...	1
42Fv125_I	300 × 300	5.27 ± 0.19	2.09 ± 0.04	...	...	1
42Fv125_II	90 × 60	5.15 ± 0.17	1.97 ± 0.03	...	...	1
42Fw9	310 × 280	5.16 ± 0.27	1.54 ± 0.05	...	...	1
			Other silicates			
34A-4	390 × 310	4.15 ± 1.17	3.16 ± 0.34	16 ± 22	64 ± 26	4
34A-6	230 × 190	5.85 ± 0.33	1.43 ± 0.05	...	...	1
42C-5	230 × 315	8.82 ± 0.91	1.99 ± 0.13	...	...	1
42F-13	150 × 150	31.83 ± 1.11	1.68 ± 0.08	...	...	1
42Fe14	220 × 180	5.73 ± 0.26	1.83 ± 0.04	...	...	1
42Ff16	320 × 160	5.40 ± 0.29	1.82 ± 0.05	...	...	1
42Fs4_I	360 × 160	6.40 ± 0.21	1.75 ± 0.03	...	...	1
42Fs4_II	280 × 210	5.84 ± 0.24	1.97 ± 0.05	...	...	1
42Fu7	400 × 280	7.92 ± 0.30	1.91 ± 0.05	...	...	1
42Fv113	220 × 210	5.48 ± 0.30	1.70 ± 0.05	...	...	1
			Oxides			
34C-6	150 × 190	7.39 ± 0.49	2.03 ± 0.08	...	...	1
42Fb3	190 × 90	6.04 ± 0.44	1.56 ± 0.07	...	...	1
42Ff26	270 × 120	7.31 ± 0.42	1.98 ± 0.06	...	...	1
42Fs6	200 × 120	7.09 ± 0.27	1.34 ± 0.04	...	...	1

Notes. Errors are 1σ.
[a] Classification into groups based on Nittler et al. (1997).

3.2. Elemental Compositions

All 48 presolar grains were characterized in the Auger Nanoprobe via elemental spectra and high-resolution maps. Figure 3 shows an example of an undifferentiated and differentiated Auger spectrum of the presolar ferromagnesian silicate grain 42Fb2 (size ∼160 × 120 nm^2). Cesium was implanted in the sample during NanoSIMS measurements and appears as a

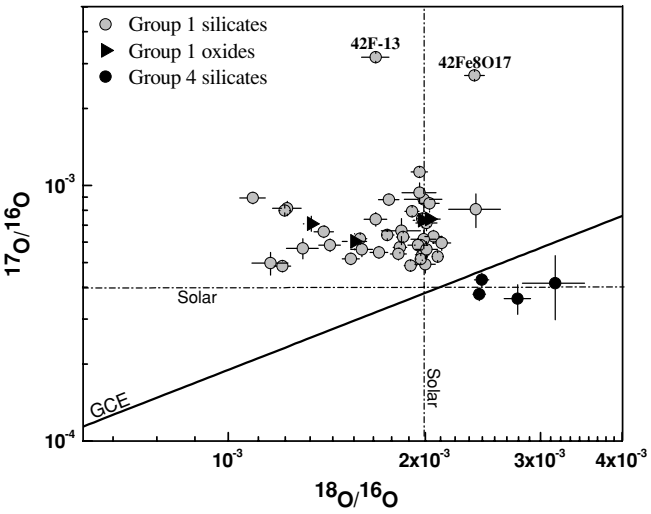

Figure 1. Oxygen three-isotope plot of presolar silicates (circles) and oxides (triangles) identified in Acfer 094. Silicate grains are classified into group 1 (gray symbols) and group 4 (black symbols) based on their O isotopic groups defined by Nittler et al. (1997). The dashed lines represent solar values. The solid line labeled "GCE" indicates the expected evolution of O isotopic ratios with increasing metallicity (Timmes et al. 1995). Errors are 1σ.

complex peak, at around 572 eV in the spectrum. The elemental compositions of the 44 silicate and 4 oxide grains are listed in Table 2, along with the Mg+Fe(+Ca)/Si and (Mg/Mg+Fe) $\times$ 100 (mg#) ratios. Grains containing O, Fe, and Mg (with or without Al, Ca, and Si) with mg#s less than 45 are considered Fe-rich and those with mg#s greater than 55 are considered Mg-rich. Grains are classified as either olivine-like or pyroxene-like if their Mg+Fe(+Ca)/Si ratios fall within 1σ of the theoretical ratios of 2 for olivine $(Mg,Fe)_2SiO_4$ and 1 for pyroxene $(Mg, Fe)SiO_3$.

Twelve grains have Mg+Fe(+Ca)/Si ratios with pyroxene-like compositions and six grains have olivine-like compositions (Figure 4). Since O is not included in the Mg+Fe(+Ca)/Si ratio, but must also be present in stoichiometric proportions, two additional ratios, namely cation/O and O/Si, were evaluated. These ratios can provide additional verification of whether the classification of a silicate grain is consistent with olivine or pyroxene and can identify grains that do not contain O in stoichiometric proportions. The classification of three olivine-like and six pyroxene-like silicate grains is less certain based on these criteria; these grains are marked with asterisks in Table 2 and Figure 4. A large number of grains (16 out of 40) have Mg+Fe(+Ca)/Si ratios intermediate between 1 and 2 (1.3–1.7; Figure 4). Finally, ten grains have Mg+Fe(+Ca)/Si ratios that are either significantly lower than 1 or higher than 2; these are listed under the category of "Other Silicates" in Table 2.

Silicate grains that are olivine-like include one grain, 42Fw3, with a forsterite (i.e., Mg-rich end-member) composition (Figure 5). The other olivine-like grains have elevated Fe concentrations (mg#s ranging from 17 to 31). Among the pyroxene-like silicates, one grain, 42Fs13, has an enstatite-like composition. However, the majority of pyroxene-like grains are Fe-rich with mg#s from 27 to 40, including two grains that have compositions that are consistent with Fe-rich end-member pyroxene and fall in the "forbidden zone" of the pyroxene quadrilateral

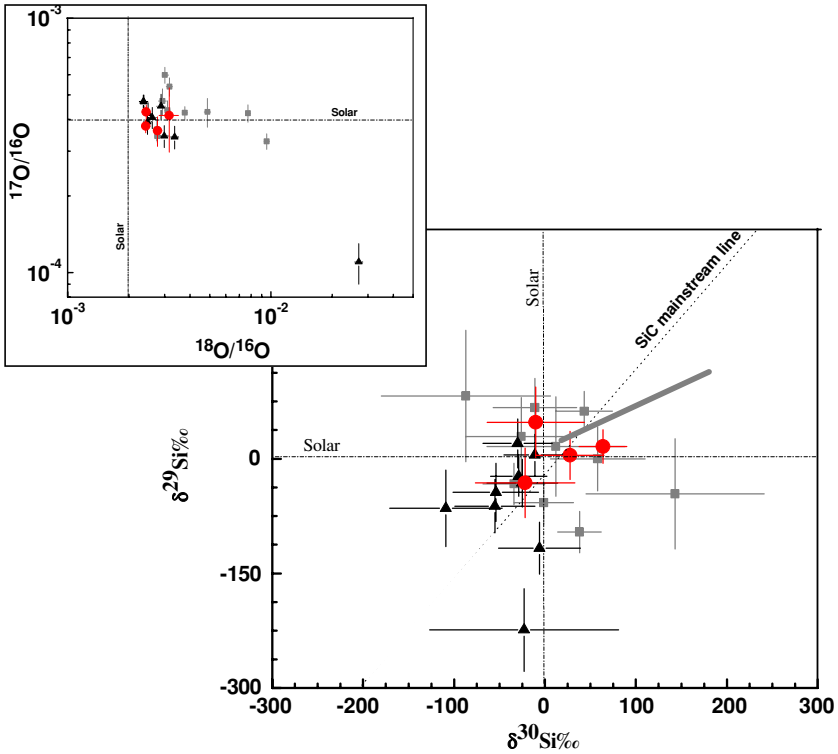

Figure 2. Silicon three-isotope plot in delta notation shows the compositions of group 4 presolar grains identified in this study (circles). Mixing calculations were also performed for ten grains (squares) from the literature (Mostefaoui & Hoppe 2004; Bland et al. 2007; Yada et al. 2008; Floss & Stadermann 2009). Additional group 4 grains from Vollmer et al. (2008) and Messenger et al. (2005) are plotted as triangles. Calculated Si isotopic ratios based on mixing of material from the H envelope to the He/C and O/C zones are represented by the thick gray line. Also shown for reference is the SiC mainstream line (slope = 1.37). The inset shows the O isotopic compositions of these grains using identical symbols. Error bars are 1σ.

(A color version of this figure is available in the online journal.)

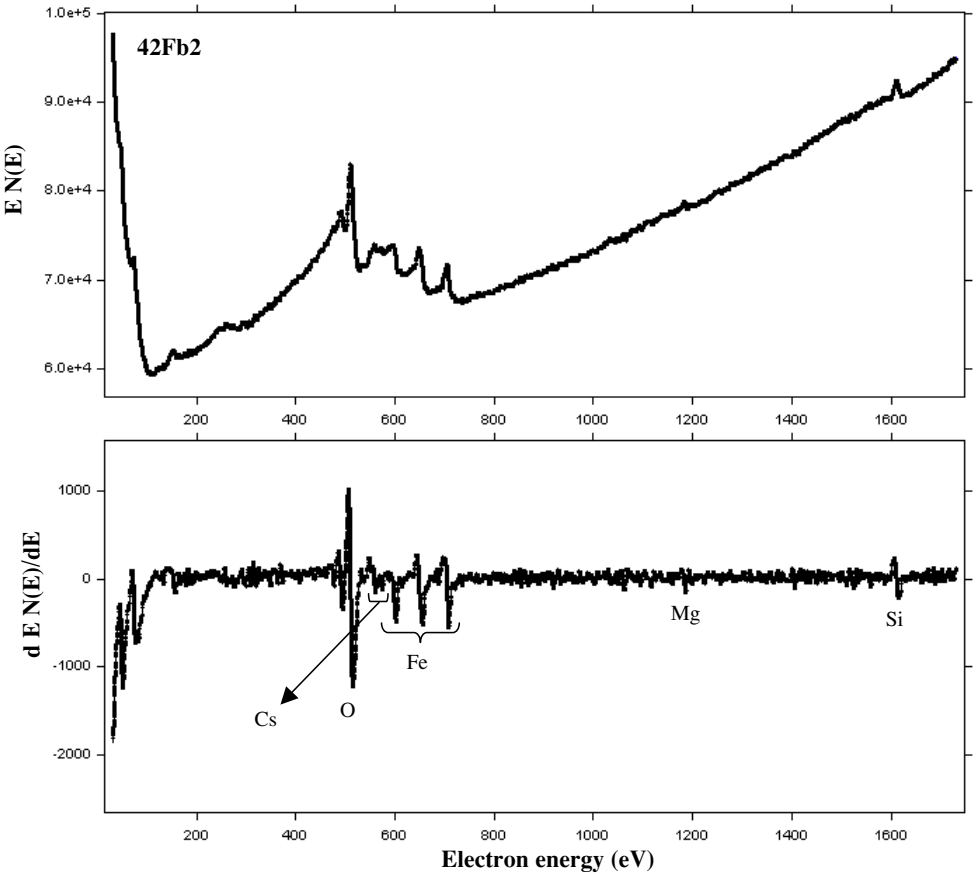

Figure 3. Auger elemental spectrum of presolar ferromagnesian silicate grain 42Fb2 with intermediate composition ($1 < \mathrm{Mg+Fe(+Ca)/Si} < 2$). The undifferentiated spectrum is shown in the top panel and the same spectrum after smoothing and performing a seven-point Savitsky–Golay differentiation is shown in the bottom panel. The elements present in the grain are also indicated.

(Deer et al. 1992, p.145). None of the pyroxene-like grains contain Al and only one grain contains Ca.

The majority of the silicate grains that have intermediate Mg+Fe(+Ca)/Si ratios are also Fe-rich. Two of these intermediate silicates have non-stoichiometric Fe-rich end-member compositions. A few grains in this category contain small detectable amounts of Ca (1.8–5.7 at.%) in addition to O, Fe, Mg, and Si. The exact classification of individual grains as olivine- or pyroxene-like on the basis of elemental ratios is accompanied by significant uncertainties, but the study of the statistical distributions of various grain types is much more robust. Olivine and pyroxene grain standards cluster around their expected Mg+Fe(+Ca)/Si ratios of 2 and 1, respectively (Stadermann et al. 2009), yet a number of standard grains have Mg+Fe(+Ca)/Si ratios between 1 and 2. Thus, it is possible that some of the silicate grains with intermediate compositions belong to either the olivine- or pyroxene-like categories. However, the number of such grains in our study is significantly larger than what is expected statistically if the inventory was only comprised of olivine and pyroxene grains, indicating that most of the intermediate grains represent a distinct group.

Six of the ten presolar grains labeled "Other Silicates" in Tables 1 and 2 contain Ca and/or Al along with Fe and Mg. Three of these grains, 34A-6, 42F-13, and 42Fv113, are Al-rich with only the first two exhibiting very high Mg+Fe(+Ca)/Si ratios. One grain, 42Fe14, is rich in Si with an O/Si ratio of 1.8 ± 0.2 and contains only minor amounts of Fe and Mg. Two other grains (42Fs4_I & 42Fs4_II) also have Si-rich compositions with O/Si ratios of $\sim$2. Eight grains classified as "Other Silicates" contain more Fe than Mg (mg# $\leqslant$ 40) and two grains show no detectable Mg at all. Grain 42C-5 has the highest Fe content (47.1 ± 5.3 at.%) among all the presolar silicate grains characterized in this work. Finally, grain 42Fu7 has Mg+Fe(+Ca)/Si, cation/O, and O/Si ratios that are only slightly outside the 1σ range for pyroxene.

Among the four oxides, two grains, 34C-6 and 42Fs6, contain Al, Fe, and Mg, one grain, 42Fb3, is spinel-like and the final grain, 42Ff26, is probably a TiO_2 grain (O/Ti = 1.9; Figure 6). Quantification of the Ti-oxide spectrum was done using a sensitivity factor for Ti determined from a TiO standard, which suggests a Ti concentration of 34 at.% in the grain. The Ti error was calculated by assuming a relative uncertainty of 10% (Table 2).

4. DISCUSSION

4.1. Group 1 Grains

A majority of the silicate and oxide grains (44 out of 48) identified in the grain size separates of Acfer 094 are group 1 grains, rich in ^{17}O and with close-to-solar or sub-solar ^{18}O/^{16}O ratios (e.g., Nittler et al. 1997). When a star runs out of H fuel in its core, it expands, cools, and undergoes an episode of deep convection called the first dredge-up, which mixes material from the deep layers of the star into the envelope, thus changing its composition (Boothroyd & Sackmann 1999). This mixing brings CNO products of partial H-burning to the surface. The CNO cycle produces ^{17}O but destroys ^{18}O, and as

Table 2
Elemental Compositions of Presolar Silicate and Oxide grains along with Mg+Fe(+Ca)/Si ratio and mg#

Grain	Si (at.%)	Al (at.%)	Fe (at.%)	Mg (at.%)	Ca (at.%)	O (at.%)	Ti (at.%)	Mg+Fe(+Ca)/Si	mg#
Pyroxene-like silicates									
42Ff11O18	21.7 ± 2.4	...	21.5 ± 2.4	...	...	56.8 ± 2.0	...	1.0 ± 0.2	0
42Ff25O	22.2 ± 2.4	...	14.3 ± 1.6	7.6 ± 0.7	...	55.9 ± 2.0	...	1.0 ± 0.1	35
42Fs13	20.3 ± 2.2	...	...	20.8 ± 2.0	...	58.9 ± 2.1	...	1.0 ± 0.1	100
42Ft13	19.1 ± 2.1	...	13.0 ± 1.5	8.7 ± 0.8	...	59.2 ± 2.1	...	1.1 ± 0.2	40
42Ft14_I	17.6 ± 1.9	...	15.9 ± 1.8	5.7 ± 0.5	...	60.8 ± 2.2	...	1.2 ± 0.2	27
42Ft24	22.9 ± 2.5	...	16.3 ± 1.8	6.1 ± 0.6	...	54.7 ± 2.0	...	1.0 ± 0.1	27
34C-7*	26.7 ± 2.9	...	7.9 ± 0.9	17.4 ± 1.6	...	48.0 ± 1.7	...	0.9 ± 0.1	69
42C-7*	30.5 ± 3.4	...	22.1 ± 2.5	12.5 ± 1.2	...	34.9 ± 1.3	...	1.1 ± 0.2	36
42Fe8O18*	24.8 ± 2.7	...	11.9 ± 1.3	14.8 ± 1.4	...	48.5 ± 1.7	...	1.1 ± 0.1	55
42Ff2*	22.9 ± 2.5	...	24.9 ± 2.8	...	...	52.2 ± 1.9	...	1.1 ± 0.2	0
42Ff12*	24.9 ± 2.7	...	13.6 ± 1.5	8.5 ± 0.8	...	53.1 ± 1.9	...	0.9 ± 0.1	38
42Fv114_I*	27.8 ± 3.1	...	14.0 ± 1.6	6.3 ± 0.6	4.5 ± 0.5	47.4 ± 1.7	...	0.9 ± 0.1	31
Olivine-like silicates									
42Fc3	14.3 ± 1.6	...	24.8 ± 2.8	6.1 ± 0.6	...	54.8 ± 2.0	...	2.2 ± 0.3	20
42Fs8	15.5 ± 1.7	...	22.0 ± 2.5	8.2 ± 0.8	...	54.4 ± 2.0	...	1.9 ± 0.3	27
42Fw3	13.7 ± 1.5	...	...	27.0 ± 2.5	...	59.3 ± 2.1	...	2.0 ± 0.3	100
42B-11*	22.0 ± 2.4	...	37.8 ± 4.2	14.0 ± 1.3	...	26.2 ± 0.9	...	2.3 ± 0.3	27
42Ft21*	16.6 ± 1.8	...	28.6 ± 3.2	6.1 ± 0.6	...	48.7 ± 1.8	...	2.1 ± 0.3	17
42Fu5*	19.9 ± 2.2	...	24.2 ± 2.7	10.9 ± 1.0	...	44.9 ± 1.6	...	1.8 ± 0.2	31
Intermediate silicates									
34C-5	23.8 ± 2.6	...	17.9 ± 2.0	7.4 ± 0.7	5.7 ± 0.6	45.3 ± 1.6	...	1.3 ± 0.2	29
42B-1	23.3 ± 2.6	...	15.4 ± 1.7	16.8 ± 1.6	...	44.5 ± 1.6	...	1.4 ± 0.2	52
42F-11	25.1 ± 2.8	...	29.0 ± 3.2	10.2 ± 1.0	...	35.7 ± 1.3	...	1.6 ± 0.2	26
42Fb2	17.1 ± 1.9	...	24.2 ± 2.7	5.1 ± 0.5	...	53.6 ± 1.9	...	1.7 ± 0.2	17
42Fd6	20.6 ± 2.3	...	21.0 ± 2.4	8.2 ± 0.8	...	50.2 ± 1.8	...	1.4 ± 0.2	28
42Fe2	20.0 ± 2.2	...	19.7 ± 2.2	9.2 ± 0.9	...	51.2 ± 1.8	...	1.4 ± 0.2	32
42Fe5O17	18.8 ± 2.1	...	15.4 ± 1.7	10.7 ± 1.0	1.8 ± 0.2	53.4 ± 1.9	...	1.5 ± 0.2	41
42Fe8O17	18.1 ± 2.0	...	20.5 ± 2.3	6.7 ± 0.6	...	54.7 ± 2.0	...	1.5 ± 0.2	25
42Fe13	17.6 ± 1.9	...	15.7 ± 1.8	13.5 ± 1.3	...	53.2 ± 1.9	...	1.7 ± 0.2	46
42Ff3	17.8 ± 2.0	...	16.9 ± 1.9	8.1 ± 0.8	4.5 ± 0.5	52.7 ± 1.9	...	1.7 ± 0.2	32
42Ff5	16.9 ± 1.9	...	23.4 ± 2.6	...	...	59.6 ± 2.1	...	1.4 ± 0.2	0
42Ff10	20.8 ± 2.3	...	29.8 ± 3.3	...	...	49.4 ± 1.8	...	1.4 ± 0.2	0
42Fv115	18.2 ± 2.0	...	22.2 ± 2.5	...	2.5 ± 0.3	57.2 ± 2.1	...	1.4 ± 0.2	0
42Fv125_I	18.5 ± 2.0	...	19.7 ± 2.2	8.5 ± 0.8	...	53.4 ± 1.9	...	1.5 ± 0.2	30
42Fv125_II	18.9 ± 2.1	...	22.9 ± 2.6	4.5 ± 0.4	...	53.7 ± 1.9	...	1.4 ± 0.2	16
42Fw9	18.4 ± 2.0	...	9.7 ± 1.1	18.0 ± 1.7	...	54.0 ± 1.9	...	1.5 ± 0.2	65
Other silicates									
34A-4	12.3 ± 1.3	7.6 ± 1.9	26.2 ± 2.9	7.5 ± 0.7	1.5 ± 0.2	44.9 ± 1.6	...	2.9 ± 0.4	22
34A-6	5.7 ± 0.6	23.2 ± 5.8	16.1 ± 1.8	8.7 ± 0.8	1.2 ± 0.1	45.2 ± 1.6	...	4.6 ± 0.6	35
42C-5	18.1 ± 2.0	...	47.1 ± 5.3	11.3 ± 1.1	...	23.5 ± 0.8	...	3.2 ± 0.5	19
42F-13	5.9 ± 0.6	22.8 ± 5.7	19.4 ± 2.2	4.6 ± 0.4	2.1 ± 0.2	45.3 ± 1.6	...	4.4 ± 0.6	19
42Fe14	29.7 ± 3.3	...	9.3 ± 1.0	6.0 ± 0.6	...	54.9 ± 2.0	...	0.5 ± 0.1	39
42Ff16	10.3 ± 1.1	7.5 ± 1.9	28.3 ± 3.2	3.2 ± 0.3	1.6 ± 0.2	49.1 ± 1.8	...	3.2 ± 0.5	10
42Fs4_I	26.5 ± 2.9	...	11.3 ± 1.3	4.8 ± 0.5	...	57.3 ± 2.1	...	0.6 ± 0.1	30
42Fs4_II	27.0 ± 3.0	...	16.0 ± 1.8	...	...	57.0 ± 2.1	...	0.6 ± 0.1	0
42Fu7	22.7 ± 2.5	...	9.4 ± 1.0	6.1 ± 0.6	3.5 ± 0.4	58.3 ± 2.1	...	0.8 ± 0.1	40
42Fv113	18.8 ± 2.1	19.7 ± 4.9	14.4 ± 1.6	...	...	47.0 ± 1.7	...	0.8 ± 0.1	0
Oxides									
34C-6	...	22.9 ± 5.7	27.0 ± 3.0	8.0 ± 0.8	...	42.2 ± 1.5	...	...	23
42Fb3	...	22.3 ± 5.6	...	13.8 ± 1.3	...	63.9 ± 2.3	...	...	100
42Ff26	...	...	...	...	...	65.8 ± 2.4	34.3 ± 3.4	...	...
42Fs6	...	22.7 ± 5.6	13.2 ± 1.5	8.7 ± 0.8	...	55.4 ± 2.0	...	...	40

Notes. mg# = Mg/(Fe+Mg) × 100. Errors are 1σ.

a result, in the first dredge-up the $^{17}O/^{16}O$ ratio of the surface increases drastically and the $^{18}O/^{16}O$ ratio decreases slightly, relative to the initial composition of the star. For stars with masses between 1 and 2.5 $M_{\odot}$, the $^{17}O/^{16}O$ ratio increases with increasing mass but it decreases in stars that are more massive (Boothroyd et al. 1994; Boothroyd & Sackmann 1999). The $^{18}O/^{16}O$ ratio, however, is not a function of mass but depends primarily on the initial metallicity of the parent star. These predictions are in reasonable agreement with O isotopic ratios that have been measured spectroscopically in evolved stars (e.g.,

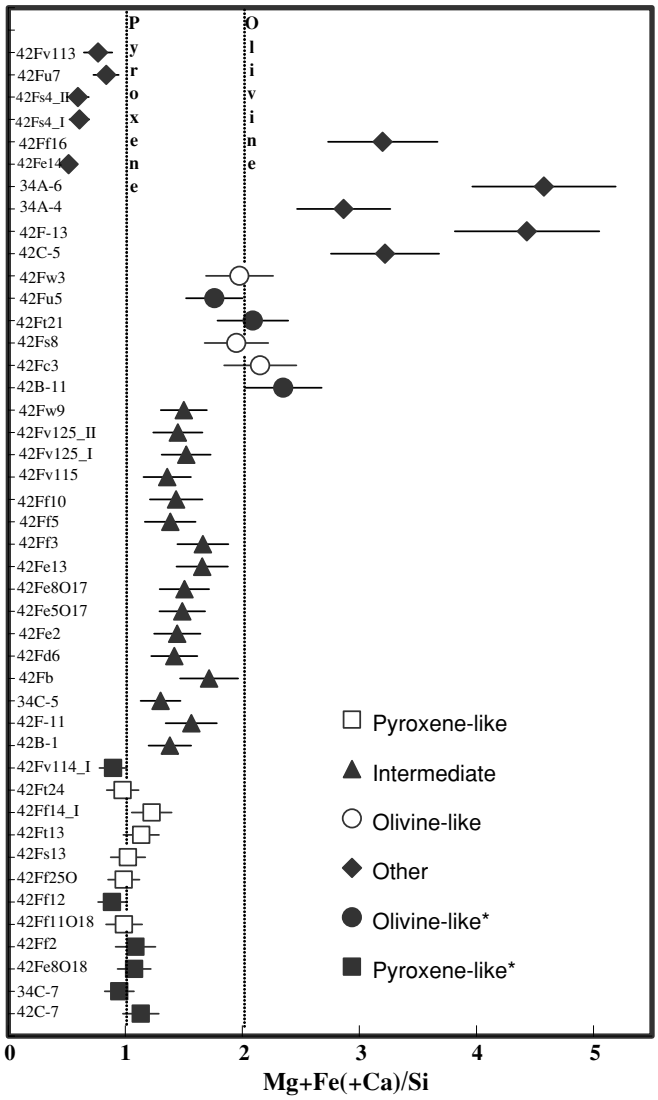

Figure 4. Plot of Mg+Fe(+Ca)/Si ratios in presolar ferromagnesian silicates. The dashed lines indicate theoretical ratios for olivine and pyroxene. Olivine-like grains and pyroxene-like grains whose cation/O and O/Si ratios are non-stoichiometric are indicated by "closed symbols" and are marked with an asterisk (*) in Tables 1 and 2.

Harris et al. 1988). All the group 1 silicate grains found in this study have compositions consistent with an origin in low-mass RG and AGB stars with near solar metallicities. Copious amounts of silicate dust can form in stars with initial masses $>$ 4 $M_{\odot}$ that undergo third dredge-up (Gail et al. 2009). However the O-isotopic composition of silicate grains from such stars should exhibit $^{17}O/^{16}O > 0.002$–0.004 (Nittler 2009), which is rarely observed for silicate grains, including ones identified in this study. Two ferromagnesian silicate grains, 42F-13 and 42Fe8O17, are characterized by higher $^{17}O/^{16}O$ isotopic ratios than the other group 1 grains (Figure 1), but are still well below the maximum $^{17}O/^{16}O$ ratios predicted for first dredge-up in stars of near solar metallicity (Nittler et al. 2008).

Modeling by Nguyen et al. (2007) has shown that ion imaging measurements of tightly packed grains in the NanoSIMS are diluted by the surrounding isotopically normal silicates, resulting in measured isotopic compositions that are closer to solar values than the intrinsic compositions of the grains. While this dilution affects all measured compositions, the effect is most pronounced for grains with compositions that are depleted in

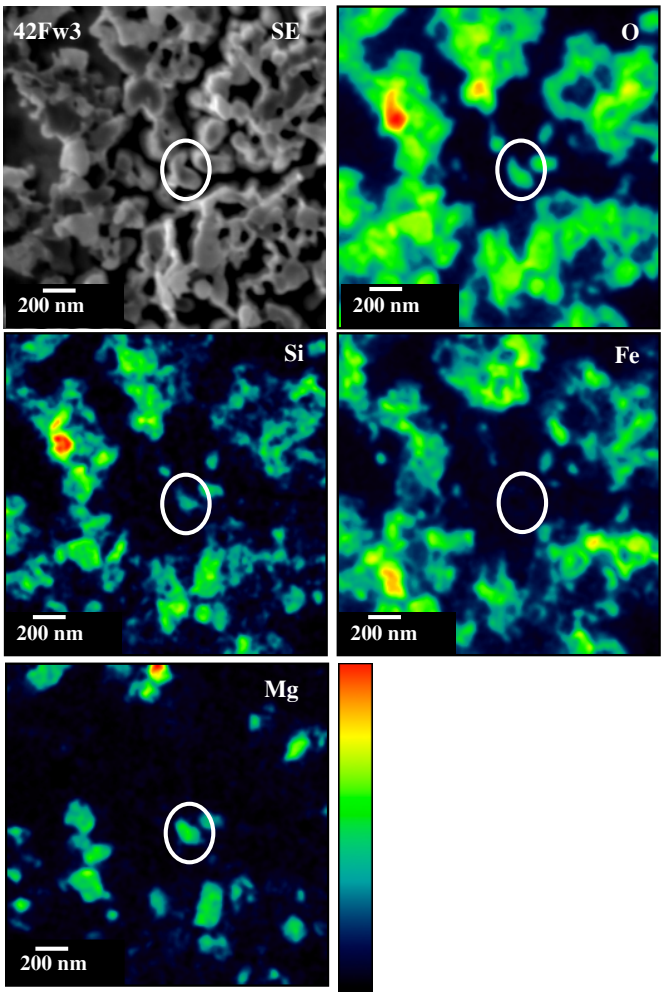

Figure 5. False color Auger elemental maps and SE image of presolar silicate grain 42Fw3, which has a forsterite-like composition.

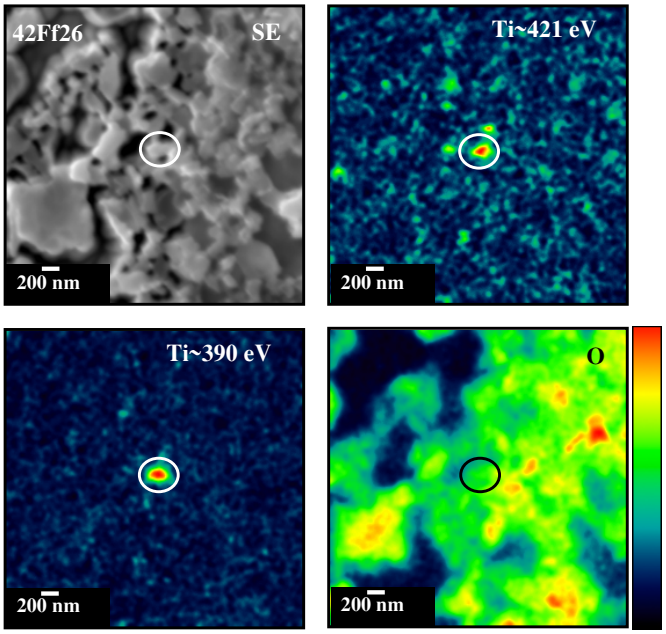

Figure 6. False color Auger elemental maps and SE image of TiO_2 grain. Titanium has two Auger peaks at about 390 and 421 eV; hotspots appear at both the energies in the false colored map.

the low-abundance isotopes relative to solar, such as the ^{18}O-depleted group 2 grains (Nittler et al. 1997). Because of this dilution effect, some of our group 1 grains with $^{18}O/^{16}O$ ratios close to 10^{-3} (e.g., 42B-1) may actually belong to group 2. Large ^{18}O depletions in group 2 grains indicate that they probably formed in low-mass AGB stars (1.2–1.8 $M_{\odot}$) undergoing cool bottom processing (Wasserburg et al. 1995; Nollett et al. 2003). Cool bottom processing, also referred to as "deep mixing," occurs when material from the envelope circulates down into the radiative zone above the H shell, and rapidly brings up nuclear processed material. The processed material is devoid of ^{18}O that has been rapidly destroyed, via the reaction ^{18}O (p, α) ^{15}N.

Our oxide grain population contains a presolar TiO_2 grain (42Ff26) with a solar $^{18}O/^{16}O$ ratio and a $^{17}O/^{16}O$ ratio that is 1.9 times the solar value. Individual presolar Ti oxide grains have previously been identified in residues of several meteorites (Nittler et al. 2008). Three group 1 Ti oxide grains found by Nittler et al. (2008) have close-to-solar Ti isotopic ratios. Titanium isotopes are affected by neutron capture reactions and small shifts in the Ti abundances are predicted to occur after third dredge-up in low-mass AGB stars (Zinner et al. 2007). However, we are not able to acquire Ti isotopic data for the TiO_2 grain found in this study due to the small size (270 × 120 nm^2) of this grain (Figure 6) and the fact that Ti isotopic measurements in the NanoSIMS need to be made with an O^- primary beam, which has a spatial resolution of no better than 300 nm.

Another group 1 oxide grain 42Fb3 has a spinel-like ($MgAl_2O_4$) composition with an Al/Mg ratio of 1.6 ± 0.4. Abundant presolar spinel grains have been identified in acid residues from meteorites including Tieschitz, Bishunpur, and Semarkona (Nittler et al. 1994, 1997, 2008; Choi et al. 1998). Most of these spinels have O isotopic compositions that are consistent with theoretical values obtained from models of O-rich RG or AGB stars (e.g., Lugaro et al. 2007). Several authors (e.g., Choi et al. 1998; Zinner et al. 2005) have reported variable Al/Mg ratios of presolar spinel grains determined from NanoSIMS isotopic measurements, suggesting that these grains may be non-stoichiometric. However, the Auger measurement of grain 42Fb3 shows that it is, within errors, consistent with stoichiometric spinel. Transmission electron microscopy (TEM) analysis of another presolar spinel, UOC-S2, also indicates a stoichiometric composition (Zega et al. 2009). It remains unclear whether most presolar spinels tend to be non-stoichiometric or whether the variable ratios are due to SIMS matrix effects. Spinel grains form in the envelopes of AGB and RG stars as a result of a solid–gas interaction of Al_2O_3 with gaseous Mg (Lodders & Fegley 1999) and condensation of our spinel grain may have occurred via such a process. Finally, the O isotopic compositions of the remaining two oxide grains, 34C-6 and 42Fs6 are also compatible with an AGB source.

4.2. Group 4 Grains

In this study, four silicate grains (Table 1) show ^{18}O enrichments and normal Si isotopic compositions (within 2σ; Figure 2). Elemental analyses of the four grains indicate that two have Fe-rich end-member compositions, including one with a pyroxene-like stoichiometry. The remaining grains have Fe-rich ferromagnesian compositions, one with an olivine-like stoichiometry, while the other is non-stoichiometric and contains Al and Ca.

Several possible stellar sources have been suggested for group 4 grains: early dredge-up events in evolved stars (Nittler et al. 1997), high-metallicity stars (Nittler et al. 1997), and SN explosions (e.g., Choi et al. 1998; Nittler et al. 2008). In the first scenario, the production of ^{18}O occurs via the $^{14}N + \alpha$ reaction during He-burning and the ^{18}O-rich material is brought up to the stellar surface during third dredge-up events, which occurs before ^{18}O is destroyed in later pulses. However, AGB models do not predict the occurrence of third dredge-up during the earliest thermal pulses, as is required to produce large surface enhancements in ^{18}O (Nittler et al. 2008) and, therefore, our group 4 grains probably did not form by this process. The high $^{18}O/^{16}O$ ratios of our group 4 grains could also reflect the initial ratios of high metallicity parent stars. Galactic chemical evolution (GCE; Figure 1) predicts that the abundances of the heavier isotopes (e.g., ^{17,18}O relative to ^{16}O) increase over time and, therefore, lead to higher metallicities (Timmes et al. 1995). Similarly, Si isotopes of grains that condense in higher metallicity stars should exhibit ^{29,30}Si enrichments relative to ^{28}Si and evolve along the SiC mainstream line (Figure 2). Therefore, grains condensing in high-metallicity stars should exhibit high $^{17,18}O/^{16}O$ and $^{29,30}Si/^{28}Si$ isotopic ratios. If the very high $^{18}O/^{16}O$ ratios of our grains are due to GCE, this would imply a parent star with metallicity several times higher than solar. Aside from the fact that such stars are exceedingly rare and probably were even more so at the time of solar system formation, such stars are also expected to have high $^{17}O/^{16}O$ ratios, both because of GCE and the first dredge-up. Moreover, an enrichment in ^{29,30}Si would also be expected. However, none of the ^{18}O-rich group 4 grains identified in this work show correlated excesses in ^{17}O. In addition, all the grains exhibit normal Si isotopic ratios (within 2σ). Thus, the group 4 grains from this study probably did not originate in high-metallicity stars.

Finally, an origin in an SN environment has been used to explain the compositions of several group 4 grains (e.g., Choi et al. 1998; Messenger et al. 2005). Grains that condense from the debris of a core-collapse SN may contain material from different zones of a pre-SN star. Recently, Nittler (2007) showed that it was possible to reproduce the compositions of some group 4 grains by mixing material from the H-envelope with contributions from the He/C zone, which is ^{18}O-rich, and the inner O-rich zones (O/Si, O/Ne, and O/C). We attempted to reproduce the O isotopic compositions of the group 4 grains found in this study by using this mixing model to see how this would affect the Si isotopes of the same grains. A comparison with the observed compositions could provide additional constraints about these grains' provenance. The O and Si isotopic abundances in the zones of a 15 $M_{\odot}$ pre-SN star (Rauscher et al. 2002), specifically model s15a28c, were used to model the compositions of the four group 4 grains identified in this work (Table 3). The O and Si isotopic abundances of the different zones are shown in Figure 7. These mixing calculations were also carried out for ten group 4 grains from Mostefaoui & Hoppe (2004), Bland et al. (2007), Yada et al. (2008), and Floss & Stadermann (2009). The average O isotopic ratios from each of the five zones (H-envelope, He/C, O/Si, O/Ne, and O/C) were mixed in different proportions to achieve the measured O isotopic compositions of the grains. An additional constraint for the condensation of O-rich dust grains, that the carbon content in the gas should be less than the oxygen content, i.e., C/O < 1, was also satisfied. All O isotopic compositions could be reproduced by mixing 92%–99% material from the H envelope

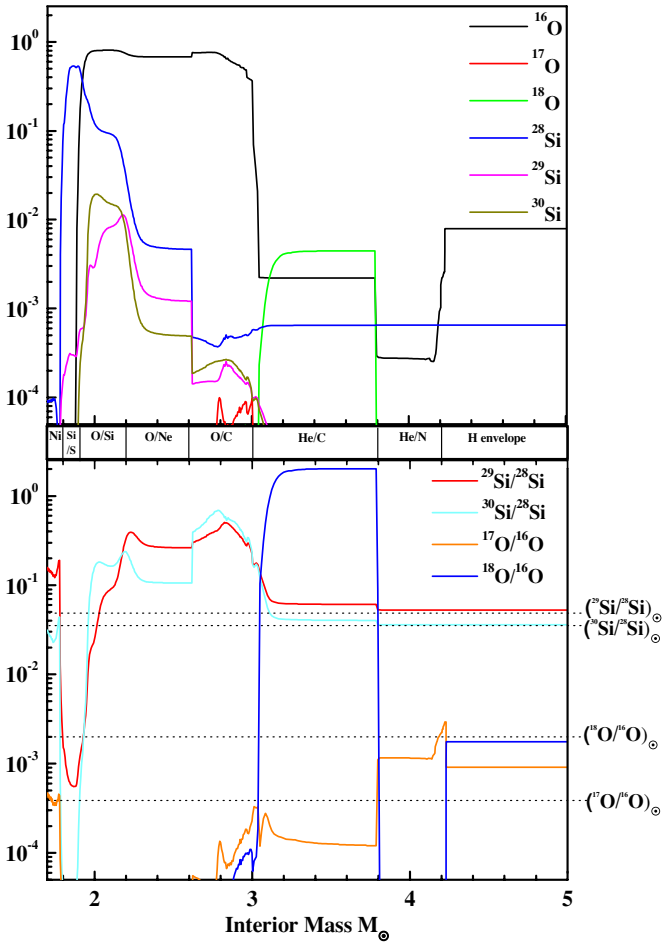

Figure 7. Oxygen and Si isotopic abundances (top) as well as $^{17,18}O/^{16}O$ and $^{29,30}Si/^{28}Si$ isotopic ratios (bottom) as a function of stellar mass in a 15 $M_\odot$ pre-SN star (Rauscher et al. 2002). The different zones in the star are labeled in the middle panel. Solar O and Si isotopic ratios are shown as dotted lines.

Table 3
Mass Boundaries of the Zones and Range of Mass Fraction

Zone	Mass Range ($M_\odot$)	Mix Fraction Range (%)	
		All Five Zones	Three Zones
H envelope	4.23–12.61	92.0–99.0	92.0–98.0
He/C	3.05–3.80	1.0–1.9	0.6–3.4
O/C	2.63–3.05	0.8–2.0	0.6–2.7
O/Ne	2.19–2.63	0.8–2.0	
O/Si	1.92–2.19	0.8–2.0	

and considerably less material from the O-rich zones and the He/C zone (Table 3). A small amount (1%–1.9%) of material from the ^{18}O enriched He/C zone is sufficient to account for the observed ^{18}O anomalies.

We then assumed that the Si isotopic ratios were mixed in the same proportions as the O isotopes and calculated the predicted Si compositions of the grains. However, using the same mixing ratios results in predicted δ^{29}Si and δ^{30}Si values that range from +87‰ to +207‰ and +425‰ to +1035‰, respectively, significantly higher than those measured in the grains. This is a reflection of the fact that the O-rich zones are also Si-rich and are enriched in the heavy isotopes of Si (Figure 7). Thus, including even small amounts of material from the O-rich zones alters the $^{29}Si/^{28}Si$ and $^{30}Si/^{28}Si$ ratios of the resulting mixture dramatically. Clearly, this mixing model is unable to simultaneously produce the ^{18}O enrichments and the solar Si isotopic ratios of the analyzed grains. Next we tested if mixing of material from the H envelope, the He/C zone, and only the O/C zone (which has the lowest Si abundance of the three O-rich zones) could explain the O and Si isotopic compositions of the 14 group 4 grains. In this case, the predicted Si isotopic ratios fall on the broad gray line in Figure 2, in qualitative agreement with almost all of the grain data, indicating that it may indeed be possible to obtain close-to-normal Si isotopic ratios with this SN mixing model.

Several group 4 silicate grains studied elsewhere (Messenger et al. 2005; Bland et al. 2007; Vollmer et al. 2008) were found to be ^{29}Si-depleted (Figure 2) and their compositions cannot be explained by either of the mixing models discussed here. One of these group 4 silicates shows an extreme ^{18}O isotopic enrichment, accompanied by a large ^{17}O depletion. Its formation was suggested to have occurred as a result of the mixing of O-rich material from the He/C and O/C zones with the Si-rich material from the Si/S and Ni zones (Messenger et al. 2005). Vollmer et al. (2008) also identified a few group 4 grains that are ^{29}Si-depleted. These authors argued for an SN origin for these grains by performing SN mixing calculations that required mixing material from six zones, including the He/N and inner ^{28}Si-rich, Si/S zones. While contributions from the inner ^{28}Si-rich Si/S zone are required to explain the Si isotopic compositions of the ^{29}Si-depleted group 4 grains, the compositions of the four grains from our study can be reproduced with contributions from only the several SN zones described above.

4.3. Silicon-rich, Silicon-poor & Aluminum-rich Grains

Three group 1 grains (42Fe14, 42Fs4_I, & 42Fs4_II) have Si-rich compositions. Two grains are ferromagnesian silicates while one grain contains no Mg at all (Table 2). The formation of Si-rich phases is possible under non-equilibrium conditions in low-metallicity stars with low Mg/Si ratios (Ferrarotti & Gail 2001). However, stars with low metallicities exhibit low $^{18}O/^{16}O$ ratios. The $^{18}O/^{16}O$ ratios of our grains are too high i.e., greater than $(1.75 \pm 0.03) \times 10^{-3}$ to have originated in low-metallicity stars, even if we consider substantial dilution of the isotopic ratios (e.g., Nguyen et al. 2007). Moreover, it is questionable whether dust grains can form under such low metallicity conditions at all (Gail et al. 2009). Nagahara & Ozawa (2009) concluded that Si-rich phases may condense in kinetically fractionating systems where the condensation of Fe metal onto forsterite prevents the equilibration of Si-rich gas with the forsterite to produce enstatite, thereby allowing the formation of Si-rich grains.

Four ferromagnesian grains (34A-4, 34A-6, 42F-13, and 42Ff16) that exhibit Al and Ca Auger peaks in their spectra have Si-poor compositions given by Mg+Fe(+Ca)/Si ratios of ~2.9–4.6. None of these grains resemble any stoichiometric Al- and/or Ca-bearing mineral phases. All the grains exhibit Fe-rich compositions with mg#s from ~10 to 35. Another grain (42Fv113) is similar with respect to the high Al contents (~23 at.%), but has a lower Mg+Fe(+Ca)/Si ratio. Abundant presolar Al_2O_3 grains have been identified in acid residues of meteorites (e.g., Nittler et al. 1994, 1997). Aluminum oxide is predicted to be the first condensate to form in an O-rich circumstellar environment (Lodders & Fegley 1999). As temperatures decrease, Al_2O_3 can act as a nucleation site for the subsequent condensation of ferromagnesian silicates (Gail & Sedlmayr 1999) or can react with the gas to form Al-bearing silicates. The "complex" silicate grains containing

Al-rich subgrains (>200 nm) identified by Vollmer et al. (2009b) provide evidence for the former process. The Al-bearing silicate grains from our study may be products of the latter scenario, in which the influence of kinetics is significant, resulting in non-stoichiometric compositions. Grain 34A-4 is a group 4 grain and may have condensed under non-equilibrium conditions in SN ejecta, where a sharp drop in temperature resulting in the incorporation of Fe into the condensing grains may result in the formation of ferromagnesian silicate minerals (Gail & Sedlmayr 1999; Ferrarotti & Gail 2001; Gail 2003).

4.4. Olivine- and Pyroxene-like Grains

Both amorphous and crystalline silicates have been discovered around young main sequence stars (Waelkens et al. 1996; Malfait et al. 1998) as well as O-rich AGB stars (Waters et al. 1996; Demyk et al. 2000). Demyk et al. (2000) suggest that the broad stellar spectral features of amorphous silicates primarily indicate olivine-like compositions, with pyroxene-like compositions being relatively rare (<10%). On the other hand, enstatite appears to be much more abundant than forsterite among crystalline silicates (Molster et al. 2002). Grains with pyroxene-like compositions are twice as abundant as olivine-like grains in our inventory. The (Mg+Fe)/Si ratios of the majority of silicate grains identified by Vollmer et al. (2009b) in Acfer 094 scatter around a value of 1, which also indicates an over-abundance of pyroxene-like grains compared to olivine-like compositions. Although Auger spectroscopy does not provide structural information about the phases and, therefore, we do not know whether the grains are crystalline or amorphous, the higher proportion of pyroxene-like grains may suggest that some grains are crystalline (e.g., Molster et al. 2002). However, the Fe high contents of many of these grains (see Section 4.5) may indicate that they are amorphous, as astronomical observations suggest that crystalline silicates are Mg-rich (Demyk et al. 2000). Stoichiometric presolar silicates in the CR3 chondrites QUE 99177 and MET 00426 consist of approximately equal numbers of olivine-like and pyroxene-like grains (Floss & Stadermann 2009), which suggests that the apparent over-abundance of pyroxene-like grains in Acfer 094 may be simply a statistical effect. To date, only a small fraction of presolar silicates have been analyzed using TEM. A few of these silicate grains are crystalline circumstellar grains with olivine compositions (Messenger et al. 2003, 2005); Vollmer et al. (2007) also found an unusual presolar silicate in Acfer 094 with a perovskite structure. However, the majority of presolar silicate grains studied in the TEM are heterogeneous on the scale of ∼20–50 nm, have overall non-stoichiometric compositions, and amorphous structures (Nguyen et al. 2007; Vollmer et al. 2009a; Stroud et al. 2008, 2009). Therefore, it is possible that most of the silicate grains are indeed amorphous.

Shocks, irradiation, and sputtering processes in the ISM may alter the structure and composition of crystalline dust grains (e.g., Lodders & Amari 2005). For example, Demyk et al. (2001) showed that crystalline olivine can transform into amorphous pyroxene when irradiated by low-energy He^+ ions. Such an irradiation process is probably responsible for the low abundance of crystalline silicates in the ISM and the transition from olivine grains around evolved stars to pyroxene grains around protostars (Demyk et al. 2001). The large number of grains with pyroxene-like compositions in our study may have resulted from such a process in the ISM. Amorphous silicate grains with stoichiometries in-between olivine and pyroxene may also be the result of irradiation and sputtering events

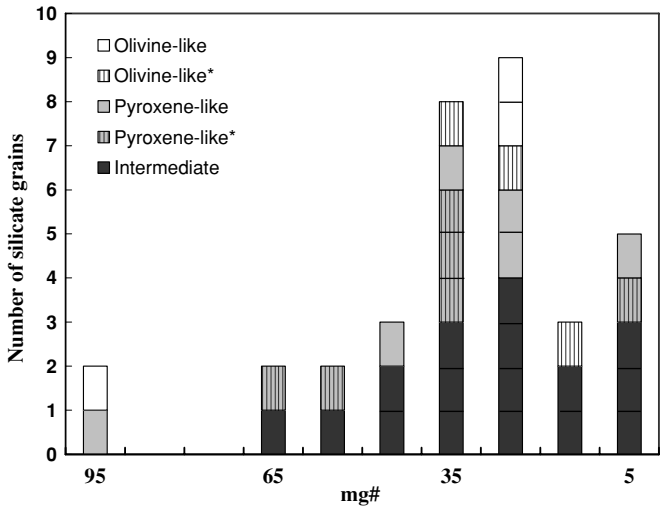

Figure 8. Histogram displaying the Fe–Mg distributions in presolar olivine-like, pyroxene-like, and intermediate silicates. Categories correspond to those shown in Figure 4.

(Jones 2000; Min et al. 2007). A large fraction of the silicates found in this study have elemental compositions intermediate between olivine and pyroxene (Figure 4). However, Min et al. (2007) predict the existence of Mg-rich grains (mg#s > 90) with stoichiometry between olivine and pyroxene in the ISM, which is in sharp contrast to the Fe-rich compositions of the grains in our inventory.

4.5. Iron-rich Silicate Grains

Figure 8 shows the distribution of mg#s for olivine- and pyroxene-like silicates, as well as for grains with compositions intermediate between these two stoichiometries. Silicates with high Fe/Mg ratios dominate our presolar grain inventory. The addition of the oxide grains or the "other" silicate grains does not change the distribution substantially. Relatively Fe-rich presolar silicate grains have been previously reported in Acfer 094 (Nguyen & Zinner 2004; Nguyen et al. 2007; Vollmer et al. 2009b), as well as in the CR3 chondrites, QUE 99177 and MET 00426 (Floss & Stadermann 2009), and the CO3 chondrite, ALHA77307 (Nguyen et al. 2008; Bose et al. 2009). The possible origin of these Fe-rich silicates is discussed in the following sections.

4.5.1. Primary Processes: Condensation in Stars

Equilibrium condensation models predict that silicates with Mg-rich end-member compositions, such as forsterite and enstatite, are the first silicate minerals to condense at high (∼1000 K) temperatures in stellar envelopes (Lodders & Fegley 1999; Ferrarotti & Gail 2001; Gail 2003). Although earlier studies had suggested higher Fe contents in amorphous silicates (e.g., Molster et al. 2002; Demyk et al. 2000), recent models using realistic particle shapes suggest that amorphous silicate grains are more Mg-rich (mg# > 90) than previously assumed (Min et al. 2007). In addition, the best fit to the scattered emission spectra from interstellar dust requires an Mg:Fe abundance of ∼2–3.6 (Costantini et al. 2005). A viable primary mechanism that may produce Fe-rich silicates is non-equilibrium condensation of grains occurring in the outflows of stars. The dusty gas in stars is lost rapidly by radiation pressure, resulting in a sharp drop in temperature in which equilibrium may not be maintained, allowing a considerable fraction of Fe to be incorporated into condensing silicate grains (Gail & Sedlmayr 1999;

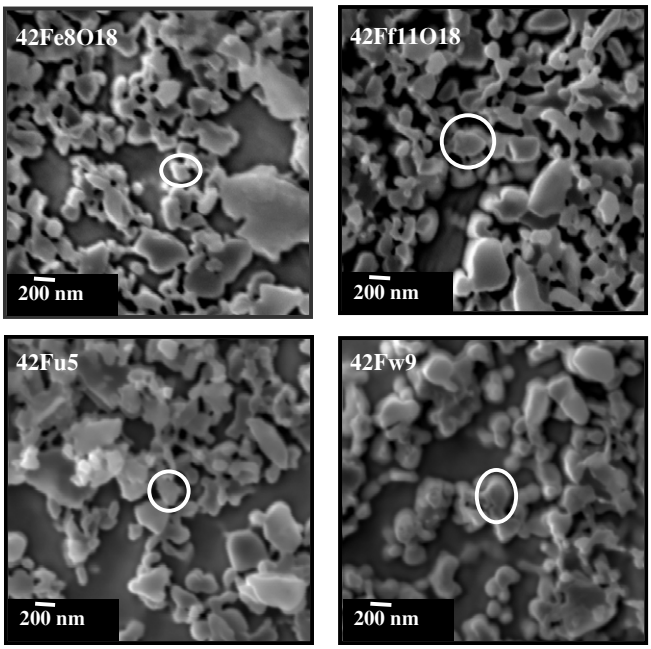

Figure 9. Field emission SE Auger images of presolar ferromagnesian silicates with compact grain morphologies.

Ferrarotti & Gail 2001; Gail 2003). In such a non-equilibrium environment, a large fraction of Mg may condense into other solid phases (e.g., Ferrarotti & Gail 2001). Evidence for the incorporation of Fe into silicates in circumstellar environments has also been obtained from laboratory experiments carried out to understand non-equilibrium condensation of silicates (e.g., Rietmeijer et al. 1999; Nuth et al. 2000). These laboratory experiments show that condensates with ferrosilica and magnesiosilica compositions form directly from the vapor, but that grains with FeMgSiO compositions are not among the primary condensates (Rietmeijer et al. 1999). Thus, silicates with Fe-rich end-member compositions, such as those found in this study, may have formed under similar circumstances. Rietmeijer et al. (1999) suggest further that dust aggregates form by accretion of simple end-member silicates, which then undergo energetic reactions and result in the formation of grains with ferromagnesian silicate compositions. High-resolution SE images of the silicate grains from our study (Figure 9) show a predominance of silicate grains with single complete grain boundaries with uniform O isotopic and elemental compositions, unlike the aggregates expected from such a process. However, the physical separation procedure carried out to produce the grain size separates could have resulted in the preferential survival of larger and more compact grains. Aggregates such as those postulated by Rietmeijer et al. (1999) have been observed in TEM studies, which show that many presolar silicates exhibit composite structures with heterogeneous elemental distributions (e.g., Stroud et al. 2009; Vollmer et al. 2009a).

One consequence of non-equilibrium condensation is the formation of olivine as the dominant mineral species rather than pyroxene (Ferrarotti & Gail 2001). The apparent conflict with the observation of more pyroxene-like compositions among our grains may be due to possible transformation in the ISM, as discussed above.

4.5.2. Secondary Processes

Secondary processes such as aqueous alteration or thermal metamorphism could also be responsible for the relatively high Fe contents in the circumstellar silicates from this study. The changes that occur at various stages of aqueous alteration include hydration of matrix material, oxidation of Fe-Ni metal, and formation of carbonates (Brearley 2006). Recently, Vollmer et al. (2009b) reported cracks and fissures in several presolar silicate grains in Acfer 094, which they attributed to aqueous alteration. However, apart from small amounts of phyllosilicate minerals, such as serpentine and chlorite, found in the matrix of Acfer 094, secondary phases, such as carbonates, are scarce in this meteorite which, in general, exhibits little evidence of aqueous alteration (Greshake 1997).

Thermal metamorphism, leading to the introduction of Fe via diffusion (e.g., Jones & Rubie 1991) could also account for the high Fe contents observed in our presolar silicate grains. Carbon-rich grains (∼100 nm in size) located within the fine-grained matrix of Acfer 094 have probably undergone limited graphitization by mild heating in the solar nebula (Brearley 2008). However, Raman measurements on insoluble organic matter (IOM) show that the Acfer 094 parent body did not experience significant thermal metamorphism (Busemann et al. 2007). In addition, Kimura et al. (2006) argued that the Fe–Ni metal in Acfer 094 shows very little plessitic intergrowth, another indicator for a low degree of metamorphism experienced by the parent body.

Changes in elemental compositions can occur in the grains during erosional processes in the ISM, which preferentially remove Si compared to Mg, and both Mg and Si compared to Fe (Jones 2000), resulting in Fe-rich grain compositions. In this case, the timescales for which the circumstellar grains remain in the ISM is crucial, e.g., cosmic ray exposure ages of large presolar SiC grains vary from ∼10 Myr to ∼1 Gyr (e.g., Ott & Begemann 2000; Gyngard et al. 2009). Most of these refractory SiC grains show no signs of processing in the ISM such as sputtering or cratering, despite their long lifetimes. Silicate grains on the other hand, are not as refractory as SiC grains, and because both SiC and silicate grains have similar long residence lifetimes in the ISM (Jones et al. 1994), preferential erosion may contribute to the high Fe contents observed in many of our silicate grains. However, preferential erosion certainly requires that the presolar grains already contain some Fe of primary origin.

Acfer 094 was found in the Algerian Sahara and is classified as W2: moderately weathered (Bischoff & Geiger 1995). The presence of ferrihydrite (∼2 mol.%) in the matrix of Acfer 094 has been attributed to alteration in the Sahara (Greshake 1997). Additional evidence for terrestrial weathering is found in the low C abundance of IOM in Acfer 094, suggesting that it was partially destroyed (Alexander et al. 2007) and in the presence of Fe^{3+}-bearing phyllosilicates (Bland et al. 2008). The degree of weathering that a hot desert meteorite experiences on the surface of the Earth has been positively correlated with its terrestrial age (Bland et al. 1996, 1998b). The terrestrial age of Acfer 094 as determined by ^{36}Cl dating is 160 ± 60 kyr (K. Nishiizumi 2008, private communication), which is longer than the residence times of many other chondritic falls (Bland et al. 1998b). Although weathering can be extremely variable in hot desert environments depending on the climatic conditions and meteorite class, most weathering occurs rapidly, probably in the first 100 years after the fall (Bland et al. 1998a), suggesting that Acfer 094 may have experienced at least some terrestrial alteration. Laboratory experiments, such as stepped combustion of chondrites (Ash & Pillinger 1995), performed to understand the weathering effects in Saharan meteorites, indicate H, C, and N elemental depletions due to the removal of

organic C. The effects of weathering may also include losses of significant Na, Mg, Si, and S from the bulk meteorite (Dreibus et al. 1993). Fayalitic olivines have greater dissolution rates than fosteritic olivines, which would suggest that the Fe-rich ferromagnesian silicate grains found in our inventory would be quickly destroyed (Wogelius & Walther 1992). On the other hand, Bland et al. (1998b) observed a decrease in Si and Mg (and minor decreases in Na and Ca) in the bulk ordinary chondritic compositions while no significant changes were observed in the Fe elemental concentrations. These authors argue that the dissolution products of ferromagnesian silicates are flushed out as weathering proceeds, except for Fe, which remains bound in hydrated Fe oxides. Assuming that carbonaceous chondrites are affected by alteration processes in a similar manner, progressive removal of certain elements, such as Mg, could contribute to the relatively high observed Fe contents in the silicate grains. The fact that such alteration does not appear to have affected other components of the bulk meteorite such as the Fe–Ni and troilite (Bland et al. 2008) may imply the involvement of only small amounts of fluid reacting preferentially with the fine-grained matrix materials.

4.5.3. Sources of Fe Enrichments

In summary, it appears that the Fe-rich presolar silicate grains from Acfer 094 probably condensed in stellar outflows under non-equilibrium conditions, followed by minimal processing in the ISM and the solar nebula, as well as some degree of terrestrial alteration. The relative contribution to the presolar grain compositions from any of these processes remains an open question. In order to constrain the primary versus secondary nature of the Fe-enrichments in presolar silicates, we have measured Fe isotopes in two grains. The Fe isotopic ratios of these grains, 42Fe14 and 42Ff11O18, did not yield any significant anomalies within 2σ errors. However, these results may have been affected by the relatively large beam size of the O^- primary beam compared to the sizes of the grains (which necessarily results in the inclusion of some surrounding matter in the analysis) and low secondary ion signals. Iron isotopic ratios have been measured in two other O-anomalous grains, to date, and both exhibit anomalous Fe isotopic compositions (Mostefaoui & Hoppe 2004; Floss et al. 2008), indicating that these grains may have acquired their isotopic compositions by primary processes occurring in stellar environments.

4.6. Silicate/Oxide Ratios

This study identified 44 presolar silicates and four presolar oxides (silicate/oxide ratio $\sim 11^{+11}_{-5}$ with 1σ errors; Gehrels 1986) in Acfer 094. The silicate/oxide ratios for the O-anomalous grains identified in other studies of the same meteorite range from 1^{+1}_{-5} to 7^{+2}_{-1} (Nguyen et al. 2007; Vollmer et al. 2009b); the latter ratio is within 1σ of the silicate/oxide ratio obtained in our work. The rather low silicate/oxide ratio obtained by Nguyen et al. (2007) may be attributed to using the NanoSIMS to ascertain whether an O-anomalous grain is a silicate or an oxide grain. Phase identification on the basis of NanoSIMS secondary ion yields alone may lead to misidentifications and subsequent errors in the silicate/oxide ratios. In contrast to the low silicate/oxide ratios in Acfer 094, a total of 53 silicates and only one oxide grain were identified in the matrices of two CR chondrites: QUE 99177 and MET 00426 (Floss & Stadermann 2009). In addition, recent Auger measurements of O-anomalous grains in the CO3 chondrite ALHA77307 show high silicate/oxide ratios from 31^{+58}_{-25} (prelim. data from our lab.) to 35^{+67}_{-29} (A. N. Nguyen 2009, private communication). Such comparisons of the presolar silicate/oxide ratios in various meteorite classes can provide a gauge for the effects of secondary processing on presolar grain survival.

The variable silicate/oxide ratios observed in the primitive meteorites studied to date can be the result of a variety of factors including local heterogeneity in the ISM, secondary alteration processes or insufficient statistics. However, it is generally thought that silicate grains are more susceptible to destruction or alteration than oxide grains (e.g., Nguyen et al. 2007; Floss & Stadermann 2009). If this is the case, and if the high ratios observed in ALHA77307 and the CR chondrites MET 00426 and QUE 99177 are indeed representative of these meteorites, then these ratios may represent the initial proportion of presolar silicate and oxide grains in the protosolar molecular cloud from which the solar system evolved. This would further imply that the lower silicate/oxide ratios in Acfer 094 are the result of secondary processing and that this meteorite is, therefore, not as primitive as previously thought. This argument is supported by the low silicate/oxide ratio (3^{+2}_{-3}) that was found from measurements of the CR chondrite NWA 530 (Leitner et al. 2009). These authors suggested that the parent body alteration experienced by NWA 530 may have destroyed a significant fraction of the silicate grains. Similarly, the low abundance of presolar silicates in the CM2 chondrite, Murchison, is probably due to aqueous alteration experienced by this meteorite (Nagashima et al. 2005). As noted above, however, the Acfer 094 matrix is almost devoid of secondary phases that form as a result of aqueous alteration (e.g., Greshake 1997). Aqueous alteration may therefore not have played a significant role in destroying silicates in this meteorite. Similarly, the low degree of heating experienced by Acfer 094 suggests that thermal metamorphism probably did not significantly affect the silicate/oxide ratios either. On the other hand, Acfer 094 does seem to have experienced some weathering on Earth leading to the presence of abundant ferric Fe in the matrix (Bland et al. 2008) and the alteration of the IOM in Acfer 094 (Alexander et al. 2007). Thus, terrestrial weathering, resulting in the destruction of silicates, could account for the low silicate/oxide ratios in this meteorite. This suggests that the silicate grain abundance calculated for Acfer 094 may be a lower limit.

5. CONCLUSIONS

The O-isotopic signatures of the 44 group 1 presolar grains found in this study reflect first and second dredge-up episodes in low-mass RG and AGB stars. Four grains with ^{18}O enrichments and normal Si isotopic ratios could have condensed in core-collapse Type II SNe. Elemental compositions acquired in the Auger Nanoprobe enabled the classification of the grains into oxides and silicates. Our presolar grain inventory contains mainly ferromagnesian silicates, some of which can be classified as olivine-like or pyroxene-like; the pyroxene-like grains are statistically more abundant. The majority of silicates are essentially Ca- and/or Al-free.

Most of the presolar silicates in this study are Fe-rich. These grains most likely originated in stellar environments controlled by non-equilibrium dust forming processes. However, the Fe enrichments observed in the grains may not solely be a primary effect. Although it is difficult to deconvolve the specific effects of terrestrial alteration and possible pre-terrestrial alteration, secondary processing may also have affected the silicate grain compositions. Additional studies of the presolar silicate populations in other meteorites may help shed more light on this ques-

tion, as stellar or ISM processes would affect all grains, while parent-body and terrestrial alterations may vary by meteorite.

Finally, the large number of non-stoichiometric silicates and the predominance of pyroxene-like over olivine-like silicates in Acfer 094 may be a result of sputtering and irradiation in shock fronts in the ISM. Indeed, collisional erosion, radiation damage, and sputtering are all expected to affect grains in the ISM on relatively short timescales.

We thank A. N. Nguyen for preparing the grain-size separates that were used in this study and Tim Smolar for maintenance of the NanoSIMS and Auger Nanoprobe. We thank the two anonymous reviewers for the detailed comments which helped improve the paper. This work was supported by NASA grants NNX07AU8OH, NNX08AI13G, and NNXO7AI82G.

REFERENCES

Alexander, C. M. O'D., Fogel, M., Yabuta, H., & Cody, G. D. 2007, Geochim. Cosmochim. Acta, 71, 4380
Amari, S., Anders, A., Virag, A., & Zinner, E. 1990, Nature, 345, 238
Ash, R. D., & Pillinger, C. T. 1995, Meteoritics, 30, 85
Bernatowicz, T., Fraundorf, G., Ming, T., Anders, E., Wopenka, B., Zinner, E., & Fraundorf, P. 1987, Nature, 330, 728
Bischoff, A., & Geiger, T. 1995, Meteoritics, 30, 113
Bland, P. A., Berry, F. J., Smith, T. B., Skinner, S. J., & Pillinger, C. T. 1996, Geochim. Cosmochim. Acta, 60, 2053
Bland, P. A., Howard, K. T., Cressey, G., & Benedix, G. K. 2008, Meteorit. Planet. Sci., 43, A26
Bland, P. A., Sexton, A. S., Franchi, I. A., Berry, F. J., & Pillinger, C. T. 1998a, Meteorit. Planet. Sci., 33, 127
Bland, P. A., Stadermann, F. J., Floss, C., Rost, D., Vicenzi, E., Kearsley, A. T., & Benedix, G. 2007, Meteorit. Planet. Sci., 42, 1417
Bland, P. A., et al. 1998b, Geochim. Cosmochim. Acta, 62, 3169
Boothroyd, A. I., Sackmann, I. J., & Wasserburg, G. J. 1994, ApJ, 430, L77
Boothroyd, A. I., & Sackmann, I. J. 1999, ApJ, 510, 232
Bose, M., Floss, C., & Stadermann, F. J. 2007, Meteorit. Planet. Sci., 42, A23
Bose, M., Floss, C., & Stadermann, F. J. 2008a, Lunar Planet. Sci. Conf., 39, Abs. 1099
Bose, M., Floss, C., & Stadermann, F. J. 2008b, Meteorit. Planet. Sci., 43, A27
Bose, M., Floss, C., & Stadermann, F. J. 2009, Meteorit. Planet. Sci., 44, A36
Brearley, A. J. 2006, Meteorites and the Early Solar System II (Tucson, AZ: Univ. Arizona Press)
Brearley, A. J. 2008, Lunar Planet. Sci. Conf., 39, Abs. 1494
Busemann, H., Alexander, C. M. O'D., & Nittler, L. R. 2007, Meteorit. Planet. Sci., 42,, 1387
Childs, K. D., Carlson, B. A., Vanier, L. A., Moulder, J. F., Paul, D. F., Stickle, W. F., & Watson, D. G. 1995, Handbook of Auger Electron Spectroscopy (3rd ed.; Eden Prairie, MN: Physical Electronics)
Choi, B.-G., Huss, G., Wasserburg, G., & Gallino, R. 1998, Science, 282, 1284
Costantini, E., Freyberg, M. J., & Predehl, P. 2005, A&A, 444, 187
Deer, W. A., Howie, R. A., & Zussman, J. 1992, An Introduction to the Rock-forming Minerals (2nd ed.; New York: John Wiley & Sons)
Demyk, K., Dartois, E., Wiesemeyer, H., Jones, A. P., & d'Hendecourt, L. 2000, A&A, 364, 170
Demyk, K., et al. 2001, A&A, 368, L38
Dreibus, G., Palme, H., Spettel, B., & Wänke, H. 1993, Meteoritics, 28, 343
Ferrarotti, A. S., & Gail, H.-P. 2001, A&A, 371, 133
Floss, C., & Stadermann, F. 2009, Geochim. Cosmochim. Acta, 73, 2415
Floss, C., Stadermann, F. J., & Bose, M. 2008, ApJ, 672, 1266
Gail, H.-P. 2003, in Astromineralogy, ed. T. Henning (Lecture Notes in Physics Vol. 609; Berlin: Springer-Verlag), 55
Gail, H.-P., & Sedlmayr, E. 1999, A&A, 347, 594
Gail, H. P., Zhukovska, S. V., Hoppe, P., & Trieloff, M. 2009, ApJ, 698, 1136
Gao, X., Amari, S., Messenger, S., Nittler, L. R., Swan, P. D., & Walker, R. M. 1996, Meteorit. Planet. Sci., 31, A48
Gehrels, N. 1986, ApJ, 303, 336
Greshake, A. 1997, Geochim. Cosmochim. Acta, 61, 437
Gyngard, F., Amari, S., Zinner, E., & Ott, U. 2009, ApJ, 694, 359
Harris, M. J., Lambert, D. L., & Smith, V. V. 1988, ApJ, 325, 768
Huss, G. R., Fahey, A. J., Gallino, R., & Wasserburg, G. J. 1994, ApJ, 430, L81
Hutcheon, I. D., Huss, G. R., Fahey, A. J., & Wasserburg, G. J. 1994, ApJ, 425, L97
Jones, A. P. 2000, J. Geophys. Res., 105, 10257
Jones, A. P., Tielens, A. G. G. M., Hollenbach, D. J., & McKee, C. F. 1994, ApJ, 433, 797
Jones, R. H., & Rubie, D. C. 1991, Earth Planet. Sci. Lett., 106, 73
Kimura, M., Weisberg, M. K., & Grossman, J. N. 2006, Meteorit. Planet. Sci., 41, 5119
Leitner, J., Hoppe, P., & Zipfel, J. 2009, Lunar Planet. Sci. Conf., 40, Abs. 1512
Lodders, K., & Amari, S. 2005, Chem. Erde, 65, 93
Lodders, K., & Fegley, B. 1999, in IAU Symp. 191, Asymptotic Giant Branch Stars, ed. T. Le Bertre, A. Lebre, & C. Waelkens (San Francisco, CA: ASP), 279
Lugaro, M., Karakas, A. I., Nittler, L. R., Alexander, C. M. O'D., Hoppe, P., Iliadis, C., & Lattanzio, J. C. 2007, A&A, 461, 657
Malfait, K., Waelkens, C., Waters, L. B. F. M., Vandenbussche, B., Huygen, E., & de Graauw, M. S. 1998, A&A, 332, L25
Messenger, S., Keller, L. P., & Lauretta, D. S. 2005, Science, 309, 737
Messenger, S., Keller, L. P., Stadermann, F. J., Walker, R. M., & Zinner, E. 2003, Science, 300, 105
Min, M., Waters, L. B. F. M., de Koter, A., Hovenier, J. W., Keller, L. P., & Markwick-Kemper, F. 2007, A&A, 462, 667
Molster, F. J., Waters, L. B. F. M., Tielens, A. G. G. M., Koike, C., & Chihara, H. 2002, A&A, 382, 241
Mostefaoui, S., & Hoppe, P. 2004, ApJ, 613, L149
Nagahara, H., & Ozawa, K. 2009, Lunar Planet. Sci. Conf., 40, Abs. 2158
Nagashima, K., Krot, A. N., & Yurimoto, H. 2004, Nature, 428, 921
Nagashima, K., Sakamoto, N., & Yurimoto, H. 2005, Lunar Planet. Sci. Conf., 36, Abs. 1671
Newton, J., Bischoff, A., Arden, J. W., Franchi, I. A., Geiger, T., Greshake, A., & Pillinger, C. T. 1995, Meteoritics, 30, 47
Nguyen, A. N. 2005, PhD Thesis, Washington Univ., Saint Louis
Nguyen, A. N., Stadermann, F. J., Nittler, L. R., & Alexander, C. M. O'D. 2008, Lunar Planet. Sci. Conf., 39, Abs. 2142
Nguyen, A. N., Stadermann, F. J., Zinner, E., Stroud, R. M., Alexander, C. M. O'D., & Nittler, L. R. 2007, ApJ, 656, 1223
Nguyen, A. N., & Zinner, E. 2004, Science, 303, 1496
Nittler, L. R. 2007, Chrono. Meteorit. Early Solar Sys., 125
Nittler, L. R. 2009, PASA, 26, 271
Nittler, L. R., Alexander, C. M. O'D., Gallino, R., Hoppe, P., Nguyen, A. N., Stadermann, F. J., & Zinner, E. K. 2008, ApJ, 682, 1450
Nittler, L. R., Alexander, C. M. O'D., Gao, X., Walker, R. M., & Zinner, E. K. 1994, Nature, 370, 443
Nittler, L. R., Alexander, C. M. O'D., Gao, X., Walker, R. M., & Zinner, E. K. 1997, ApJ, 483, 475
Nittler, L. R., Alexander, C. M. O'D., Wang, J., & Gao, X. 1998, Nature, 393, 222
Nollett, K. M., Busso, M., & Wasserburg, G. J. 2003, ApJ, 582, 1036
Nuth, J. A., Hallenbeck, S. L., & Rietmeijer, F. J. M. 2000, J. Geophys. Res., 105, 10387
Ott, U., & Begemann, F. 2000, Meteorit. Planet. Sci., 35, 53
Rauscher, T., Heger, A., Hoffman, R. D., & Woosley, S. E. 2002, ApJ, 576, 323
Rietmeijer, F. J. M., Nuth, J. A., III, & Karner, J. M. 1999, ApJ, 527, 395
Stadermann, F. J., Croat, T. K., Bernatowicz, T. J., Amari, S., Messenger, S., Walker, R. M., & Zinner, E. 2005, Geochim. Cosmochim. Acta, 69, 177
Stadermann, F. J., Floss, C., Bose, M., & Lea, A. 2009, Meteorit. Planet. Sci., 44, 1033
Stroud, R. M., Floss, C., & Stadermann, F. J. 2009, Lunar Planet. Sci. Conf., 40, Abs. 1063
Stroud, R. M., Nguyen, A. N., Alexander, C. M. O'D., Nittler, L. R., & Stadermann, F. J. 2008, Meteorit. Planet. Sci., 43, A148
Timmes, F. X., Woosley, S. E., & Weaver, T. A. 1995, ApJS, 98, 617
Vollmer, C., Brenker, F. E., Hoppe, P., & Stroud, R. M. 2009a, ApJ, 700, 774
Vollmer, C., Hoppe, P., & Brenker, F. E. 2008, ApJ, 684, 611
Vollmer, C., Hoppe, P., Brenker, F. E., & Holzapfel, C. 2007, ApJ, 666, L49
Vollmer, C., Hoppe, P., Stadermann, F. J., Floss, C., & Brenker, F. E. 2009b, Geochim. Cosmochim. Acta, 73, 7127
Waelkens, C., et al. 1996, A&A, 315, L245
Wasserburg, G. J., Boothroyd, A. I., & Sackmann, I. J. 1995, ApJ, 447, L37
Waters, L. B. F. M., et al. 1996, A&A, 315, L361
Wogelius, R. A., & Walther, J. V. 1992, Chem. Geo., 97, 101
Yada, T., Floss, C., Stadermann, F. J., Zinner, E., Nakamura, T., Noguchi, T., & Lea, A. S. 2008, Meteorit. Planet. Sci., 43, 1287
Zega, T. J., Alexander, C. M. O'D., Nittler, L. R., & Stroud, R. M. 2009, Lunar Planet. Sci. Conf., 40, Abs. 1342
Zinner, E., Nittler, L. R., Hoppe, P., Gallino, R., Straniero, O., & Alexander, C. M. O'D. 2005, Geochim. Cosmochim. Acta, 69, 4149
Zinner, E., et al. 2007, Geochim. Cosmochim. Acta, 71, 4786